IJNAOE
©SNAK, 2015

Int. J. Nav. Archit. Ocean Eng. (2015) 7:951~963
http://dx.doi.org/10.1515/ijnaoe-2015-0066
pISSN: 2092-6782, eISSN: 2092-6790

Investigation on bragg reflection of surface water waves induced by a train of fixed floating pontoon breakwaters

Huei-Tau Ouyang, Kue-Hong Chen and Chi-Ming Tsai

Department of Civil engineering, National Ilan University, Yilan City, Taiwan

Received 9 March 2015; Revised 17 July 2015; Accepted 27 July 2015

ABSTRACT: *The water wave characteristics of Bragg reflections from a train of fixed floating pontoon breakwaters was studied numerically. A numerical model of boundary discretization type was developed to calculate the wave field. The model was verified by comparing to analytical data in literature and good agreements were achieved. Series of parametric studies were conducted systematically to investigate the dependence of the reflected coefficients by the Bragg scattering on the design variables, including the spacing between the breakwaters, the total number of installed breakwaters, the draft and width do the breakwater, and wave length. Certain wave characteristics of the Bragg reflections were observed and discussed in details which might be of help for practical engineering applications in shoreline protection from incident waves.*

***KEY WORDS*:** Wave characteristics; Bragg reflection; Floating breakwaters; Surface water waves.

INTRODUCTION

It has been reported that a phenomenon namely 'Bragg reflection' would emerge as incident water waves impinge on a series of fixed structures with certain formations (Davies and Heathershaw, 1984; Mei, 1985; Cho and Lee, 2000; among many others). The incident waves and the waves reflected by the structures would be resonating which raising up the wave reflections in front of the structures. This phenomenon was first discovered by Bragg and Bragg (1913) when studied X-ray waves passing through two parallel reflective crystals. They found that the highest reflection of the X-ray emerges as the spacing between the crystals is precisely multiple of the half wave-length of the X-ray and named the reflection condition 'Bragg Law'.

The phenomenon of Bragg reflection was observed in water waves as well and has been a topical subject investigated by many researchers. Davies and Heathershaw (1984) studied water waves passing over a wavy bed by utilizing the perturbation method as an analysis tool. They showed theoretically that standing waves occur on the wavy bed when the wave-length of the bed is multiples of half of the water wave-length. They also conducted physical model experiments to verify the results. Mei (1985) showed that the sediment transport in the boundary layer of the seabed originates the dynamical mechanism for the formation of sandbars. He also showed that the sediment transport mechanism must be combined with certain standing waves in order for a sandbar to form, and Bragg reflection along the coast provides the mean to generate these standing waves. Chen (1991) solved the flow potential for water waves over a cosine-shaped bed to the second order by utilizing the perturbation method. His results showed that the strength of the wave field and the stiffness of the wave form are proportional to the ampli-

Corresponding author: *Huei-Tau Ouyang*, e-mail: *htouyang@niu.edu.tw*

tude of the wavy bed. He also showed that Bragg reflection emerges when the wave-length of the wavy bed is half of the incident wave-length. Miles (1981) derived a formula for the reflection coefficient caused by a small elevation change of the bed by adopting the linear water wave theorem. His results were then extended by Kirby and Anton (1990) to reproduce the shape of a sandbar by using Fourier Series Expansion. They also improved Miles' results by deriving a close form formula for the reflection coefficient. Hsu et al. (2002) conducted flume experiments to investigate wave reflections for three types of fictitious sandbars in shapes of rectangular, cosined, and triangular. Their results show that the rectangular sandbars produce the highest reflections among the three types of sandbars. They also found that near-full reflections could be achieved with more than 8 sandbars. Karmakar et al. (2013) studied the scattering of gravity waves by single and multiple surface-piercing floating membranes by using eigen-function expansion method to solve the wave potential. In their results, the resonating pattern in the reflection coefficient resembling the Bragg reflection was observed for multiple floating membranes.

In reviews of the above literatures on Bragg reflections of water waves, most of the focuses were on bottom structures and less has been studied on fixed floating structures. The aim of this paper is to address the focuses on this aspect. In the following, the governing equation and boundary conditions of the wave reflection problem were first introduced. A numerical model of boundary discretization type was developed and verified by comparing the results to analytical data in literature. Systematic simulations by means of the developed numerical model on the wave fields induced by various formations of fixed floating breakwater trains were performed to investigate the influence of various design variables on Bragg reflections. Notions with regards to practical applications in shoreline protection were addressed based on the results.

PROBLEM FORMULATION

A train of rigid and impermeable floating pontoon breakwters fixed on the water surface is considered, as depicted in Fig. 1. The geometric shape of the pontoon is rectangular and has a width and draft of w_f and d_f, respectively. The spacing of the breakwaters S is defined as the dsitance between the centers of two adjacent pontoons. The x-axis is along the mean sea level and the y-axis is on the vertical upward direction. Wave trains with wave height of H and frequency of σ traveling along the x-direction in water of arbitrary depth h impinge on the structures. The fluid is assumed to be invisicid, incompressible and irrotational, and the wave amplitude is small such that the linear water wave theory is applicable.

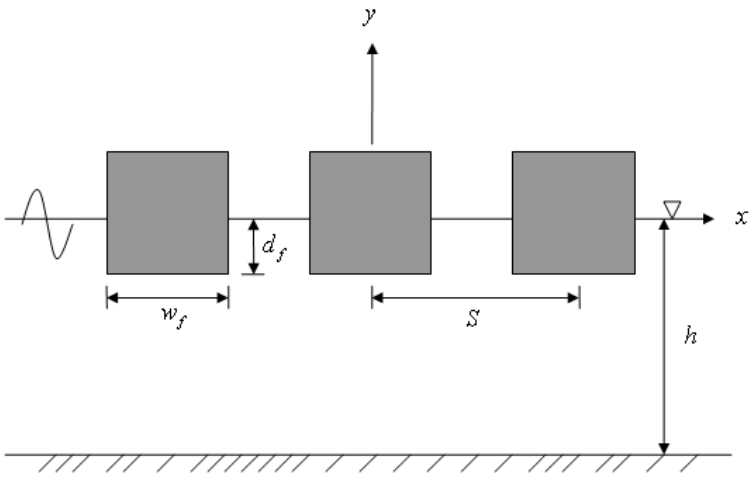

Fig. 1 Definition sketch of the floating pontoon breakwaters.

The governing equation of the wave field reads (Dean and Dalrymple, 1991)

$$\nabla^2\phi(x,y)=0 \tag{1}$$

where $\phi(x,y)$ describes the fluctuation of the potential on the x-y plane, and is related to the velocity potential of water waves as $\Phi(x,y,t)=\phi(x,y)e^{i\sigma t}$, based on the periodicity in time.

Eq. (1) is the classical Laplace equation and the solution of which is determined by the boundary conditions listed in the following.

The linearized free water surface boundary condition:

$$\frac{\partial\phi(x,y)}{\partial y}-\frac{\sigma^2\phi(x,y)}{g}=0 \tag{2}$$

Seabed and breakwater boundary conditions:

The seabed and the breakwaters are considered to be rigid and impermiable which satify the rigid boundary condition

$$\frac{\partial\phi(x,y)}{\partial n}=0 \tag{3}$$

where n is boundary normal vector.

Radiation condition at infinity:

$$\lim_{x\to\infty}\left[\frac{\partial\phi(x,y)}{\partial x}-ik\phi(x,y)\right]=0 \tag{4}$$

Boundary conditions on the fictitious interfaces:

The domain are divided into three regions by introducing two pseudo-boundaries on both sides of the structures at $x=\pm l$, as depicted in Fig. 2. The boundary conditions on the left and right pseudo-boundaries based on potential and velocity continuities are derived as follows

$$\left[\phi^{(2)}+\frac{1}{ik}\frac{\partial\phi^{(2)}}{\partial x}\right]_{x=-l}=\frac{2\cosh(k(h-y))}{\cosh(kh)} \tag{5}$$

and

$$\left[\phi^{(2)}+\frac{1}{ik}\frac{\partial\phi^{(2)}}{\partial x}\right]_{x=l}=0 \tag{6}$$

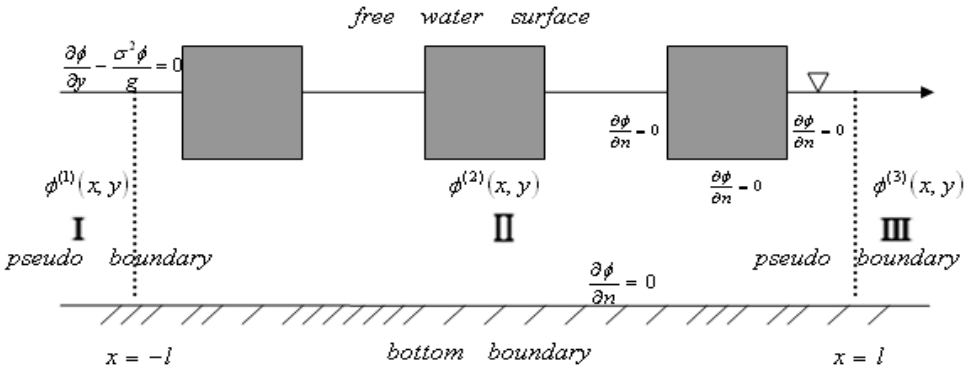

Fig. 2 Pseudo boundaries and the boundary conditions.

The reflection and transmission coefficients are also derived as follows (Chen et al., 2002)

$$R = 1 + \frac{k}{n_0 \sinh(kh)} \int_{-h}^{0} \phi^{(2)}(-l, y) \cosh k(h+y) dy \tag{7}$$

$$T = \frac{k}{n_0 \sinh(kh)} \int_{-h}^{0} \phi^{(2)}(l, y) \cosh k(h+y) dy \tag{8}$$

where $n_0 = \frac{1}{2}\left(1 + \frac{2kh}{\sinh(2kh)}\right)$

NUMERICAL MODEL

A numerical model of boundary discretization type was developed for wave field computations. The velocity potential in the wave field is simulated by a linear combination of the influences contributed by a number of source points distributed on the boundary of region *II*. The unknown coefficients for the combination of these source points can be determined by satisfying the boundary conditions listed from Eq. (2) to (6) at specific observation points (colloation points) distributed on the boundaries, as shown in the following equations.

$$\sum_{j=1}^{N} A^{(i)}(s^j, x^i) C^j = \phi(x^i), \quad x^i \in B \tag{9}$$

$$\sum_{j=1}^{N} B^{(i)}(s^j, x^i) C^j = \psi(x^i), \quad x^i \in B \tag{10}$$

where s^j and x^i are the source points and the collocation points, respectively; N is the number of these points ; B denotes the domain boundary; $\phi(x^i)$ donotes the Dirichlet BCs; $\psi(x^i) = \frac{\partial \phi}{\partial n_x}$ denotes the Neumann BCs. For mixed type boundary conditions, a linear combination of Eqs. (9) and (10) is used. C^j are the unknown coefficients to be determined; The superscript (*i*) denotes the interior domain of region *II*; Following Young et al. (2005), a Radial Basis Function satisfying the Laplace equation was employed to construct the influence coefficient $A^{(i)}(s^j, x^i)$, which reads as follows.

$$A^{(i)}(s^j, x^i) = -\frac{(x^i - s^j) \cdot n_j}{\overline{r_{ij}}^2} \tag{11}$$

From Eq. (10), it follows that $B^{(i)}(s^j, x^i) = \frac{\partial A^{(i)}(s^j, x^i)}{\partial n_x}$ and has the following form.

$$B^{(i)}(s^j, x^i) = 2\frac{((x^i - s^j) \cdot n_j)((x^i - s^j) \cdot \overline{n_i})}{\overline{r_{ij}}^4} - \frac{(n_j \cdot \overline{n_i})}{\overline{r_{ij}}^2} \tag{12}$$

where n_j and $\overline{n_i}$ are the outward normal vectors at the source point s^j and the collocation point x^i, respectively; (·) denotes the inner product; $\overline{r_{ij}} = \left|s^j - x^i\right|$ represents the distance between the source point and the collocation point.

By satisfying the appropriate boundary condition associated to each of the collocation points, Eqs. (9) and (10) lead to a system of linear equations for the unknown coefficients C^j. It is expected that C^j is to be obtained by solving the system of linear equations, and the velocity potential at any desired point within region *II* can then be obtained by substituting the now detrmined C^j into the following equation.

$$\phi(p) = \sum_{j=1}^{N} A^{(i)}(s^j, p) C^j \tag{13}$$

where p is an arbitrary point within region *II*.

Nevertheless, it is noted that the resultant linear equation system exhibits sigularities on the diagonal of the coefficient matrix. The reason for this is due to the fact that $A^{(i)}(s^j, x^i)$ and $B^{(i)}(s^j, x^i)$ are, as shown in Eqs. (11) and (12), functions of the distance between the source points and the collocation points $\overline{r_{ij}}$, which leads to singularities when $\overline{r_{ij}}$ is zero, i.e., when the location of the collocation point coincides with the source point. Special treatment has to be made to circumvent these signularities in solving the system of linear equations for C^j.

Following the subtracting and adding-back technique of Hwang et al. (2002), the sigularities in the influence matix were eliminated by utilizing the following properities (Young et al., 2005)

$$\begin{cases} A^{(i)}(s^j, x^i) = -A^{(e)}(s^j, x^i) & , i \neq j \\ A^{(i)}(s^j, x^i) = A^{(e)}(s^j, x^i) & , i = j \end{cases} \tag{14}$$

$$\begin{cases} B^{(i)}(s^j, x^i) = B^{(e)}(s^j, x^i) & , i \neq j \\ B^{(i)}(s^j, x^i) = B^{(e)}(s^j, x^i) & , i = j \end{cases} \tag{15}$$

and

$$\sum_{j=1}^{N} A^{(e)}(s^j, x^i) = 0 \tag{16}$$

$$\sum_{j=1}^{N} B^{(e)}(s^j, x^i) = 0 \tag{17}$$

where the superscript (e) denotes the exterior domain of region *II*.

The perplexing diagonal term $A^{(i)}(s^i, x^i)$ is subtracted out of Eq. (9), and instead, $A^{(e)}(s^i, x^i)$ is added-back based on the identity in Eq. (14) for $i = j$, such that Eq. (9) is revised as follows.

$$\phi(x^i) = \sum_{j=1}^{i-1} A^{(i)}(s^j, x^i) C^j + \sum_{j=i+1}^{N} A^{(i)}(s^j, x^i) C^j + A^{(e)}(s^i, x^i) C^i \tag{18}$$

It is noted that the added-back term $A^{(e)}(s^i, x^i)$ can be further replaced based on Eq. (16) and Eq. (14) as follows.

$$\begin{aligned} A^{(e)}(s^i, x^i) = -\left[\sum_{j=1}^{i-1} A^{(e)}(s^j, x^i) + \sum_{j=i+1}^{N} A^{(e)}(s^j, x^i) \right] = \\ \left[\sum_{j=1}^{i-1} A^{(i)}(s^j, x^i) + \sum_{j=i+1}^{N} A^{(i)}(s^j, x^i) \right] \end{aligned} \tag{19}$$

Substituting Eq. (19) into Eq. (18) leads to the following equation, which is a revision form of Eq. (9).

$$\phi(x^i) = \sum_{j=1}^{i-1} A^{(i)}(s^j, x^i)C^j + \sum_{j=i+1}^{N} A^{(i)}(s^j, x^i)C^j + \left[\sum_{j=1}^{i-1} A^{(i)}(s^j, x^i) + \sum_{j=i+1}^{N} A^{(i)}(s^j, x^i)\right]C^i \tag{20}$$

Similar derivation on Eq. (10) leads to the following revision of the equation.

$$\psi(x^i) = \sum_{j=1}^{i-1} B^{(i)}(s^j, x^i)C^j + \sum_{j=i+1}^{N} B^{(i)}(s^j, x^i)C^j + \left[\sum_{j=1}^{i-1} B^{(i)}(s^j, x^i) + \sum_{j=i+1}^{N} B^{(i)}(s^j, x^i)\right]C^i \tag{21}$$

It is seen in Eqs. (20) and (21) that the troublesome diagonal elements in the original influence matrix in Eqs. (9) and (10) resulting from $A^{(i)}(s^i, x^i)$ and $B^{(i)}(s^i, x^i)$ have been substituted by the summation of the other elements on a row of the matrix excluding the diagonal elements, and the resultant Eqs. (20) and (21) are thus singularity-free.

Once the singularities in the influence matrix is eliminated, the linear equation system of Eqs. (20) and (21) can be solved by standard matrix inversion technique to determine the unknown coefficient C^j. The velocity potential at any point in region *II* is then calculated by subtituting C^j into the following singularity-free revision of Eq. (13).

$$\phi(p) = \sum_{j=1}^{i-1} A^{(i)}(s^j, p)C^j + \sum_{j=i+1}^{N} A^{(i)}(s^j, p)C^j + \left[\sum_{j=1}^{i-1} A^{(i)}(s^j, p) + \sum_{j=i+1}^{N} A^{(i)}(s^j, p)\right]C^i \tag{22}$$

After solving the wave field in region *II*, the reflection and transmission coefficients can then be estimated by Eqs. (7) and (8), respectively.

NUMERICAL RESULTS AND DISCUSSIONS

The developed numerical model was verified by comparing the computational results to analytical data in literature. The model was then utilized as a numerical tool for parametric studies of the wave fields induced by various formations of floating breakwater trains.

Verification of the numerical model

Abul-Azm and Gesraha (2000) have studied wave reflections from a fixed floating pontoon by using the Eigen-Function Expansion Method (EFEM) which is considered as an analytical solution. To verify the developed numerical model, the same flow conditions in their research were employed. Fig. 3 shows the variation of the reflection coefficients *R* in region *I* obtained by the numerical model as a function of *kh* with respect to various relative widths of the breakwaters, $w_f / h =$ 0.5,1.0, and 1.5, where *h* is the water depth. For comparison, the results of Abul-Azm and Gesraha are also shown in the figure. As seen, the agreements between the numerical calculations and their results are clearly observed. The deviations of the numerical calculations from the analytical solutions are barely visible. Fig. 4 gives the comparison of the transmission coefficient *T* obtained by the numerical model with the analytical solutions. As shown in the figure, good agreements have also been achieved by the numerical model. The root mean square errors (RMSEs) in *R* and *T* of the numerical computations in comparison with the results of Abul-Azm and Gesraha are summarized in Table 1. As shown in the table, the RMSE in the refletion coefficient *R* ranges from 0.0014 to 0.0028, and from 0.0026 to 0.0074 for the transimission coefficient *T*.

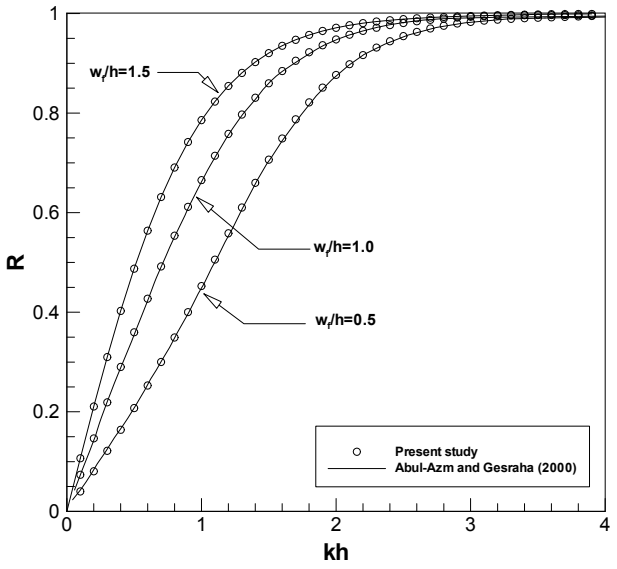

Fig. 3 Verification of reflection coefficient with respect to the relative breakwater-width ($d_f / h = 0.25$).

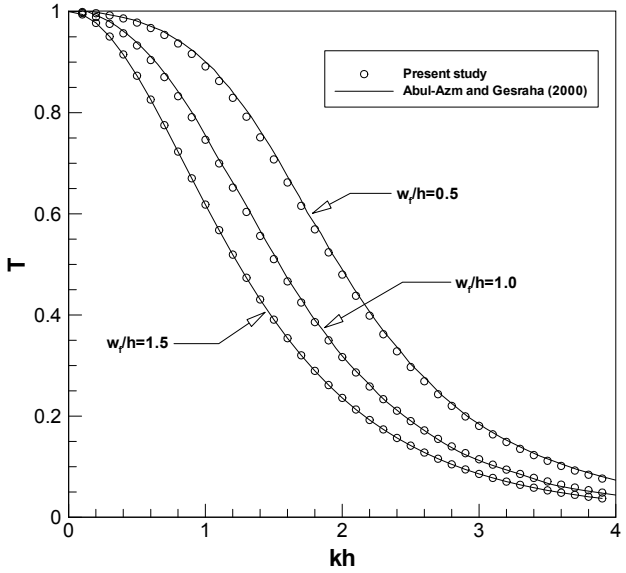

Fig. 4 Verification of transmission coefficient with respect to the relative breakwater-width ($d_f / h = 0.25$).

Table 1 Root mean square errors (RMSEs) of the numerical calculations with respect to the relative breakwater-width ($d_f / h = 0.25$).

w_f / h	0.5	1.0	1.5
RMSE (*R*)	0.0028	0.0026	0.0014
RMSE (*T*)	0.0074	0.0059	0.0026

Figs. 5 and 6 present the reflection and transmission coefficients *R* and *T* obtained by the numerical model as functions of *kh* with respect to various relative drafts of the breakwaters, d_f / h. The agreements of the numerical results with Abul-Azm and Gesraha (2000) are clearly seen in the figures. The associated RMSEs for the numerical computations are summarized in Table 1. As shown in the table, the RMSE for *R* ranges from 0.0013 to 0.0041, and from 0.0019 to 0.0078 for *T*.

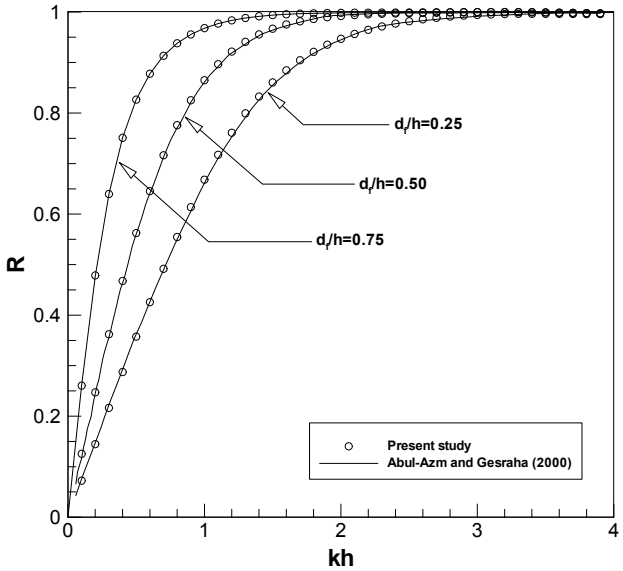

Fig. 5 Verification of reflection coefficient with respect to the relative breakwater-draft ($w_f / h = 0.25$).

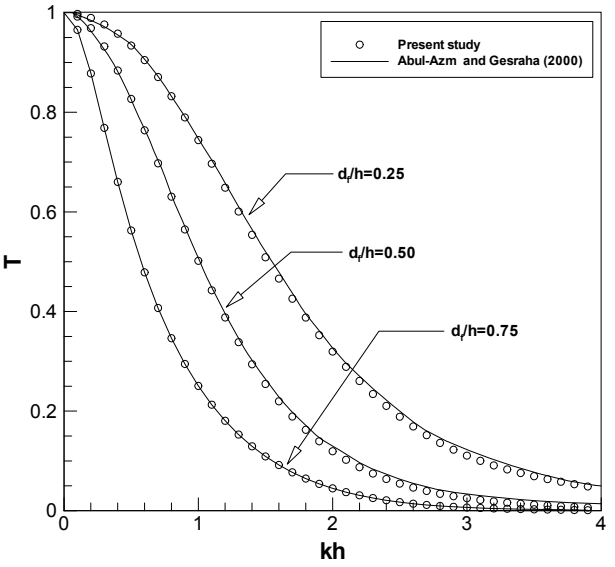

Fig. 6 Verification of transmission coefficient with respect to the relative breakwater-draft ($w_f / h = 0.25$).

Table 1 Root mean square errors (RMSEs) of the numerical calculations with respect to the relative breakwater-draft (w_f / h =0.25).

d_f / h	0.25	0.50	0.75
RMSE (*R*)	0.0041	0.0025	0.0013
RMSE (*T*)	0.0078	0.0070	0.0019

In general, the numerical model provides satisfactory results in comparison with the analytical solutions. The RMSEs of the calculated reflection and transmission coefficients subjected to various relative breakwater-widths and drafts are in general all less than 1%. The deviations would be considered acceptable in the aspect of practical engineering applications.

The Bragg reflection

It has been reported that, as a wave train with constant frequency propagates over a wavy bed or bottom breakwaters, the phenomen of Bragg reflections would emerge if the wave-length of the incident wave is approximately twice that of the bottom undulations (see for example, Cho and Lee, 2000). The incident waves and the waves reflected by the bottom undulations would resonate which raising up the reflection coefficient in front of the wavy bottom area. Extensive studies on the phenomenon of Bragg reflection have been performed experimentally and theoretically in the literature (Jeon and Cho, 2006; Elgar et al., 2003; among many others). In present study, focus is addressed on the Bragg reflections induced by a series of fixed floating breakwaters instead of bottom ones. In the following, the developed numerical model is employed to conduct a series of parametric studies in a systematic fashion to investigate the effect of the spacing between the breakwaters, the total number of installed breakwaters, the draft and width do the breakwater on Bragg reflections by a train of surface mounted pontoon breakwaters.

Number of breakwaters in a train

To investigate the influence of the total number of installed breakwaters on the reflection coefficient, series of wave fields with respect to various number of breakwaters and spacing between the breakwaters were calculated numerically. The spacing between the breakwaters *S* is measured from the centers of two adjacent breakwaters and has been normalized by half wave-length of the incident waves, i.e. 2 *S*/*L*, where *L* is the incident wave-length. Fig. 7 shows the calculated reflection coefficient *R* in region *I* as a function of 2 *S*/*L* with respect to various number of installed breakwaters N_f.

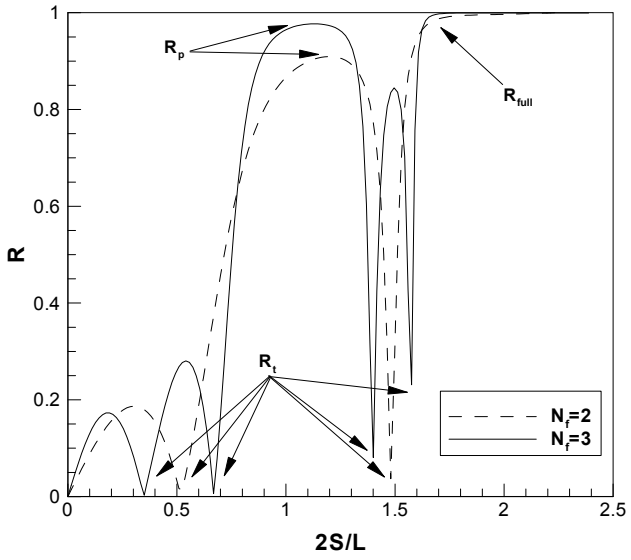

Fig. 3 Reflection coefficient as a function of relative breakwater-spacing 2 *S*/*L* with respect to the number of breakwaters in a train (d_f / h =0.25, w_f / h =0.5).

As seen in the figure, it appears that the waves reflected by the floating structure is significantly related to the relative spacing between the breakwaters. The reflection coefficient *R* varies drastically along with 2 *S*/*L*. Several prominent reflection peaks are clearly observed at certain relative breakwater-spacing 2 *S*/*L*, exhibiting the featured wave characteristics of Bragg reflections. As shown in the figure, a primary reflection peak R_p is observed as 2 *S*/*L* is about 1.0. Similar phenomenon has also been reported by Williams and Abul-Azm (1997). As seen in the figure, R_p is increasing with the number of breakwaters in a train. For N_f=2, R_p is 0.909, and for N_f=3 it is 0.977. The relative breakwater-spacing 2 *S*/*L* associated to these primary reflection peaks are in general around 1.0 yet deviate slightly for different numbers of breakwaters. For N_f =2, the primary reflection peak occurs as 2 *S*/*L* is 1.19, and for N_f=3, the relative spacing associated to the primary reflection peak is 1.11. It appears that the relative spacing of the breakwaters associated to the primary reflection peak is gradually closing to 1.0 for higher number of breakwaters.

As shown in Fig. 7, for 2 *S*/*L* around 2.0, the reflection coefficients for N_f=2 and 3 are both gradually approaching to 1.0 and the waves reach near-full reflections (R_{full}). This characteristic of wave reflections has also been reported in Williams and Abul-Azm (1997). Examination of the data shows that the reflection coefficient reaches 0.999 as 2 *S*/*L*=2.13 and 1.73 for N_f=2 and 3, respectively. It appears that the relative breakwater-spacing associated to the near-full reflection zone is gradually decreasing with more breakwaters in the train.

As shown in the figure, other than the primary reflection peak zone and the near-full reflection zone, there are also several minor reflection peaks emerging in-betweens. It is seen that the patterns of these minor reflections for N_f=2 and 3 are not the same. As 2 *S*/*L* is less than the primary reflection zone, there are 2 minor reflection peaks observed for N_f=3, yet only one is seen for N_f=2. Also, for 2 *S*/*L* intervening the primary reflection zone and the near-full reflection zone, a minor reflection peak for N_f=3 is observed, but none to be seen for N_f=2.

As shown in the figure, intervening these reflection peaks, the reflection coefficient drops down dramatically to the troughs (R_t) at certain 2 *S*/*L*, and the incident waves barely reflect for these particular relative breakwater-spacings. It is seen that, for N_f=3, the reflection coefficient drops down drastically to 0.003, 0.006, 0.080, and 0.225 for 2 *S*/*L*=0.35, 0.67, 1.40, and 1.58, respectively, and for N_f=2, the reflection coefficients fall down to 0.014 and 0.037 for 2 *S*/*L*=0.53 and 1.48, respectively.

Table 3 summarizes the reflection coefficients for the primary reflection peaks R_p and the reflection troughs R_t with the associated 2 *S*/*L* for N_f=2 and 3. As seen, wave reflections from the floating breakwater trains are strongly related to 2 *S*/*L*. The reflection coefficient exhibits significant variation from the peaks to the troughs within a rather small range of 2 *S*/*L*. It is seen that, with proper arrangement on 2 *S*/*L*, very high and even near-full reflection can be achieved. On the other hand, very low reflections can also be accomplished with certain configurations of 2 *S*/*L*. These wave characteristics might be of practical use in engineering applications. For example, high reflections would be expected when the structure is utilized as a measure for the protection of shoreline or harbor in behind from the incident waves, while low reflections would be required when the structure is adopted as a floating dock or bridge.

Table 3 Reflection coefficients for the primary reflection peaks and the reflection troughs with the associated 2 *S*/*L* (d_f/*h*=0.25, w_f/*h*=0.5).

	N_f=2				N_f=3			
2 *S*/*L*	0.53	1.19	1.48	0.35	0.67	1.11	1.40	1.58
Primary reflection peak R_p		0.909				0.977		
Reflection trough R_t	0.014		0.037	0.003	0.006		0.08	0.225

Draft of the breakwaters

Fig. 8 shows the reflection coefficient *R* in region *I* as a function of 2 *S*/*L* with respect to various drafts of the breakwaters. The draft of the breakwaters d_f has been normalized by the depth of the water, i.e., d_f/*h*, where *h* is the water depth. Several reflection peaks are clearly seen in the figure signifying the occurrence of the Bragg phenomenon. As seen in the figure, the primary peaks R_p for the three cases of d_f/*h*=0.25, 0.5 and 0.75 are all emerging around 2 *S*/*L*=1.0, which is the feature characteristic of Bragg reflections. As shown in the figure, the reflection of the incident waves is getting stronger for breakwaters with deeper draft. For d_f/*h*=0.25, R_p reaches 0.977 at 2 *S*/*L*=1.13, and for d_f/*h*=0.5 and 0.75, R_p reaches 0.999 at 2

S/L=1.06 and 0.99, respectively. Table 4 summarizes the primary reflection peaks R_p with the associated 2 S/L for various d_f/h. It appears that the associated 2 S/L for the primary reflection peak to occur is approaching 1.0 for breakwaters with deeper relative draft.

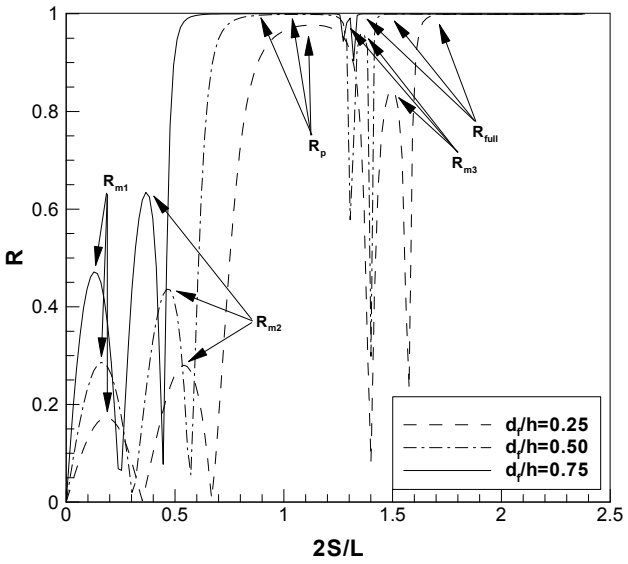

Fig. 4 Reflection coefficient with respect to the draft of the breakwaters (N_f=3, w_f / h=0.5).

Table 4 Primary reflection peaks R_p and the extents of 2 S/L for R greater than 95% of R_p with respect to the draft of the breakwaters (N_f=3, w_f/h=0.5).

	d_f/h=0.25	d_f/h=0.50	d_f/h=0.75
Primary reflection peak R_p	0.977	0.999	0.999
2 S/L for R_p	1.13	1.06	0.99
95% of R_p	0.928	0.949	0.950
Range of 2 S/L for R greater than 95% of R_p	0.92-1.29	0.70-1.27	0.51-1.27
Extent of 2 S/L for R greater than 95% of R_p	0.37	0.57	0.76

As shown in Fig. 8, the extent of 2 S/L for the primary reflection zone is also expanding with deeper d_f/h. To examine the extent of the primary reflection zone, it is defined as the area around the primary reflection peak where the reflection coefficient R is greater than 95% of the primary reflection peak R_p. Table 4 shows the extent of 2 S/L for the primary reflection zone with respect to various relative breakwater-drafts. As seen in the table, for d_f/h=0.25, the extent of 2 S/L for R greater than 95% of R_p is 0.37, and for d_f/h=0.5 and 0.75, the extents are 0.57 and 0.76, respectively. It is seen the primary reflection zone is expanding with deeper draft of the breakwaters. This wave characteristic implies that, for practical applications such as shoreline protections, breakwaters with deeper relative draft would be more advisable, since not only higher R_p can be achieved but also wider applicable extent of 2 S/L for the structure is realized.

As shown in Fig. 8, for 2 S/L greater than the primary reflection zone, a near-full reflection zone is observed. Examination of the data shows that the reflection coefficient reaches near-full reflection of 0.999 as 2 S/L greater than 1.73 for d_f/h=0.25, and 1.46 and 1.35 for d_f/h=0.50 and 0.75, respectively. It is seen that 2 S/L associated to the occurrence of the near-full reflection zone appears to decrease with deeper draft of the breakwaters.

As shown in the figure, several minor reflection peaks R_m ahead and behind the primary reflection zone are observed. Unlike the case of N_f, the patterns of these minor reflection peaks for different d_f/h are rather similar. For all the three cases of d_f/h=0.25, 0.50, and 0.75, there appear to be two minor reflection peaks emerging for 2 S/L less than the primary reflection zone,

and one minor reflection peak for 2 *S*/*L* greater than the primary reflection zone, although the one for d_f/h=0.75 is barely visible. Table 5 summarizes the reflection coefficients of these minor reflection peaks and the associated 2 *S*/*L* with respect to various drafts of the breakwaters. As seen in the table, all of the three minor reflections are increasing for breakwater trains with deeper draft, and the associated 2 *S*/*L* for the occurrence of these minor reflections are decreasing along with deeper draft.

Table 5 Reflection coefficient for the minor reflections and the associated 2 *S*/*L* with respect to the draft of the breakwaters (N_f=3, w_f/h=0.5).

	Minor reflection 1		Minor reflection 2		Minor reflection 3	
	2 *S*/*L*	R_{m1}	2 *S*/*L*	R_{m2}	2 *S*/*L*	R_{m3}
d_f/h=0.25	0.19	0.173	0.54	0.280	1.5	0.845
d_f/h=0.50	0.16	0.286	0.46	0.436	1.37	0.959
d_f/h=0.75	0.13	0.472	0.37	0.634	1.31	0.991

Width of the breakwaters

Fig. 9 shows the reflection coefficient *R* in region *I* as a function of 2 *S*/*L* with respect to various widths of the breakwaters normalized by water depth, w_f/h. The wave characteristics of Bragg reflections are clearly seen in the figure, with the featured pattern of R_p emerging at 2 *S*/*L* around 1.0. As seen in the figure, the strength of the primary reflection peak and the extent of the primary reflection zone are both increasing for breakwaters with wider relative width. Table 6 lists the reflection coefficients of the primary reflection peaks R_p with the associated relative breakwater-spacing 2 *S*/*L*, and the extents of 2 *S*/*L* for *R* greater than 95% of R_p with respect to various widths of the breakwaters. It is seen that both of R_p and the extent of 2 *S*/*L* for the primary reflection zone are increasing with w_f/h. These characteristics imply that, for practical applications where high wave reflections are expected, increasing the relative width of the breakwaters would be a viable design direction since both higher R_p and larger applicable extent of 2 *S*/*L* could be attained.

The wave reflection patterns for the three cases of w_f/h=0.40, 0.60, and 0.80 are similar, with two minor reflections in front of the primary reflection zone and one minor reflection in behind. For 2 *S*/*L* greater than the third minor reflection, a near-full reflection zone appears. The reflection coefficient reaches 0.999 for 2 *S*/*L* greater than 1.75, 1.77, and 1.81 for w_f/h=0.40, 0.60, and 0.80, respectively. It appears that 2 *S*/*L* associated to the occurrence of the near-full reflection zone is slightly increasing for breakwaters with wider width.

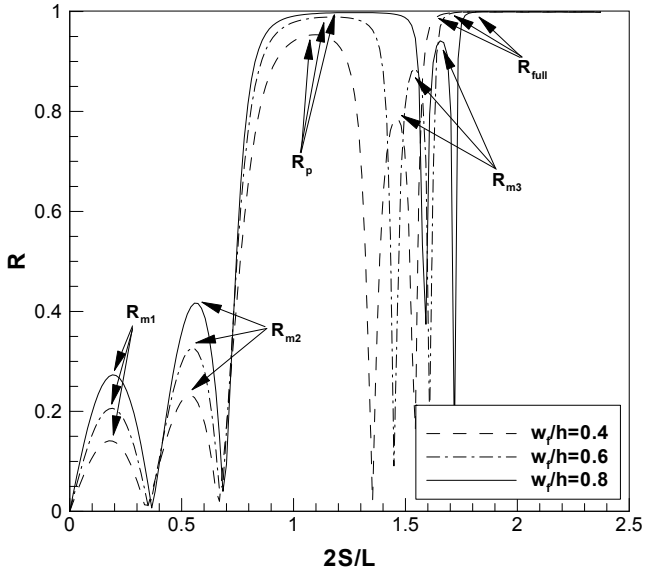

Fig. 5 Reflection coefficient with respect to the width of the breakwaters (N_f=3, d_f / h=0.25).

Table 6 Primary reflection peaks R_p and the extents of 2 S/L for R greater than 95% of R_p with respect to the width of the breakwaters (N_f=3, d_f/h=0.25).

	w_f/h=0.40	w_f/h=0.60	w_f/h=0.80
Primary reflection peak R_p	0.953	0.989	0.998
2 S/L for R_p	1.10	1.18	1.27
95% of R_p	0.905	0.940	0.948
Range of 2 S/L for R greater than 95% of R_p	0.92-1.24	0.89-1.37	0.86-0.95
Extent of 2 S/L for R greater than 95% of R_p	0.32	0.48	0.68

Table 7 summarizes the three minor reflections and the associated 2 S/L for various relative breakwater-widths. As seen in the table, the reflection coefficients for all of the three minor reflections are increasing for breakwaters with wider width. For R_{m1} and R_{m2}, the associated 2 S/L are almost the same disregarding the widths of the breakwaters. On the other hand, for R_{m3}, the associated 2 S/L is related to the width of the breakwaters and is increasing with the relative breakwater-width, as seen in the table.

Table 7 Minor reflections and the associated 2 S/L with respect to the draft of the breakwaters (N_f=3, d_f/h=0.25).

	Minor reflection 1		Minor reflection 2		Minor reflection 3	
	2 S/L	R_{m1}	2 S/L	R_{m2}	2 S/L	R_{m3}
w_f/h=0.40	0.18	0.141	0.54	0.233	1.46	0.789
w_f/h=0.60	0.19	0.206	0.54	0.326	1.54	0.886
w_f/h=0.80	0.19	0.273	0.56	0.417	1.66	0.941

CONCLUSIONS

The wave characteristics of Bragg reflections from a train of fixed floating breakwaters were investigated systematically. The results show that the Bragg reflection exhibits significant dependence on the relative spacing between the breakwaters. Two major features on wave reflection from the structure are observed, which are the emerging of the primary reflection zone and the near full reflection zone in front of the breakwaters. Simulation data shows that the primary reflection occurs as the relative spacing between the breakwaters 2 S/L is about 1.0, and the near-full reflection develops as 2 S/L is in general around 2.0. These features are in consistent with the general phenomenon of Bragg reflections reported in literature. The extents of 2 S/L associated to these two featured wave reflection zones expend with higher number of breakwaters installed and deeper relative draft of the breakwaters. Utilizing these wave characteristics of Bragg reflections by proper configurations of the floating breakwater trains, high wave reflections with large applicable extent of 2 S/L can be realized. For practical engineering applications expecting high wave reflections such as shoreline protections, these characteristics might provide informative guidelines in the preliminary design stages.

ACKNOWLEDGEMENTS

Support from the Ministry of Science and Technology in Taiwan (Grant no. 104-2626-M-197-001) is gratefully acknowledged.

REFERENCES

Abul-Azm, A.G. and Gesraha, M.R., 2000. Approximation to the hydrodynamics of floating pontoons under oblique waves.

Ocean Engineering, 27(4), pp.365-384.

Bragg, W.H. and Bragg, W.L., 1913. The reflection of X-rays by crystals. *Proceedings of the Royal Society of London*, 88, pp.428-438.

Chen, J.T., Chang, M.H., Chen, K.H. and Chen, I.L., 2002. Boundary collocation method for acoustic eigenanalysis of three-dimensional cavities using radial basis function. *Computational Mechanics*, 29(4-5), pp.392-408.

Chen, Y.Y., 1991. Analysis on progressive gravity waves over a wavy bottoms. *Journal of Harbor Technology*, 6, pp.59-83.

Cho, Y.S. and Lee, C., 2000. Resonant reflection of waves over sinusoidally varying topographies. *Journal of Coastal Research*, 16(3), pp.870-876.

Davies, A.G. and Heathershaw, A.D., 1984. Surface wave propagation over sinusoidally varying topography. *Journal of Fluid Mechanics*, 144, pp.419-443.

Dean, R.G., and Dalrymple, R.A., 1991. *Water wave mechanics for engineers and scientists*. Singapore: World Scientific.

Elgar, S., Raubenheimer, B. and Herbers, T.H.C., 2003. Bragg reflection of ocean waves from sandbars. *Geophysical research letters*, 30(1), pp.16(1)-16(4).

Hsu, T.W., Chang, H.K. and Hsieh, C.M., 2002. Bragg reflection of waves by different shapes of artificial bars. *China Ocean Engineering*, 16, pp.21-30.

Hwang, W.S., Hung, L.P. and Ko, C.H., 2002. Non-singular boundary integral formulations for plane interior potential problems. *International Journal for Numerical Methods in Engineering*, 53(7), pp.1751-1762.

Jeon, C.H. and Cho, Y.S., 2006. Bragg reflection of sinusoidal waves due to trapezoidal submerged breakwaters. *Ocean Engineering*, 33(14-15), pp.2067-2082.

Karmakar, D., Bhattacharjee, J. and Soares, C.G., 2013. Scattering of gravity waves by multiple surface-piercing floating membrane. *Applied Ocean Research*, 39, pp.158-167.

Kirby, J.T. and Anton, J.P., 1990. Bragg reflection of waves by fictitious bars. *Proceedings 22nd international conference on Coastal Engineering*, Delft, Netherlands, 2-6 July 1990, pp.757-768.

Mei, C.C., 1985. Resonant reflection of surface waves by periodic sand-bars. *Journal of Fluid Mechanics*, 152, pp.315-335.

Miles, J.W., 1981. Oblique surface-wave diffraction by a cylindrical obstacle. *Dynamics of Atmospheres and Oceans*, 6(2), pp.121-123.

Williams, A.N. and Abul-Azm, A.G., 1997. Dual pontoon floating breakwater. *Ocean Engineering*, 24(5), pp.465-478.

Young, D.L., Chen, K.H. and Lee, C.W., 2005. Novel meshless method for solving the potential problems with arbitrary domain. *Journal of Computational Physics*, 209(1), pp.290-321.